Desalination 525 (2022) 115496

Contents lists available at ScienceDirect

Desalination

journal homepage: www.elsevier.com/locate/desal

Enhancing the property of composite pervaporation desalination membrane by fabricating a less resistance substrate with porous but skinless surface structure

Dujian Qin, Hangmin Liu, Tianhui Xiong, Junli Wang, Rui Zhang *, Bing Cao *, Pei Li *

College of Materials Science and Engineering, Beijing University of Chemical Technology, Beijing 100029, China

HIGHLIGHTS

- Optimization the polysulfone (PSF) substrate to obtain a macro-void free, inter-connected pores, and skinless structure by changing the casting solution composition and the temperature of coagulation bath.
- Evaluation the composite membranes pervaporation (PV) performance and the substrate structure effect on the gas transport resistance.
- The resistance to swelling polyvinyl alcohol (PVA) layer delamination and the long-term operational stabilities of the composite membrane.
- Effects of temperature and salt concentration on the composite membranes desalination properties.
- The high-water flux PV composite membrane, with a easy-to scale-up porous substrate, demonstrated a great potential for its composite PV membrane commercialization.

GRAPHICAL ABSTRACT

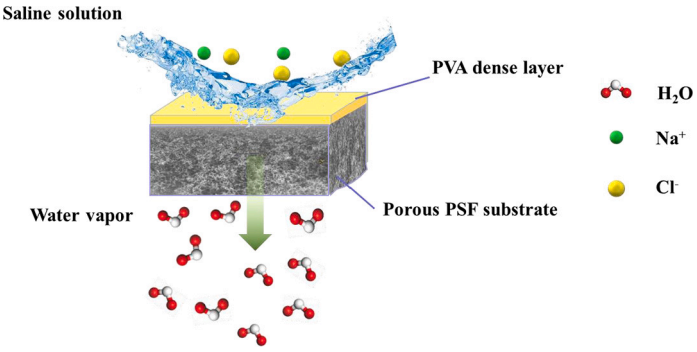

ARTICLE INFO

Keywords:
Pervaporation desalination
Non-solvent induced phase inversion
Macrovoid free and skinless cross-section
Polysulfone
Polyvinyl alcohol

ABSTRACT

The fabrication methods for high performance pervaporation (PV) desalination membranes were complicated and difficult to be scaled-up. To address this issue, we developed a composite membrane using a porous polysulfone (PSF) membrane that was prepared by a conventional non-solvent induced phase inversion (NIPS) technology. The key was to design the PSF structure with a skinless, macro-void free and bi-continuous cross-sectional morphology for achieving an ultra-low transport resistance. This was done by incorporating non-solvent additives of polyvinylpyrrolidone (PVP) and propionic acid (PA) into the PSF polymer dope and regulating the temperature of the water coagulant. As a result, the PSF based PV composite membrane exhibited a high-water flux of 124.8 ± 3.2 kg/(m^2·h) and a salt rejection of 99.9% when separating a 3.5 wt% NaCl solution at 70 °C. Moreover, a water flux of 71.3 ± 1.8 kg/(m^2·h) was achieved for treating a high concentrated NaCl solution of 20 wt%. To our best knowledge, these PV membrane desalination performances overshadowed all

* Corresponding authors.
E-mail addresses: zhangrui1@mail.buct.edu.cn (R. Zhang), bcao@mail.buct.edu.cn (B. Cao), lipei@mail.buct.edu.cn (P. Li).

https://doi.org/10.1016/j.desal.2021.115496
Received 23 September 2021; Received in revised form 1 December 2021; Accepted 6 December 2021
Available online 17 December 2021

reported PV composite membranes using substrates fabricated by the NIPs method. Most importantly, the easy-to-scale-up membrane fabrication method, as well as the excellent PV desalination performance, indicated a great potential for industrial applications.

1. Introduction

Extracting fresh water from seawater, brackish or waste waters greatly alleviate the water shortage problem world-widely [1,2]. The success lies in the high efficiency of separating water from salt or vice versa. To date, thermally based desalination technologies, such as multi-effect distillation and multi-stage flashing, have been widely applied in the middle-east regions attributing to the low price of petroleum resource [3–6]. On the other hand, seawater reverse osmosis (SWRO) technology occupies nearly 60% desalination market because of its low

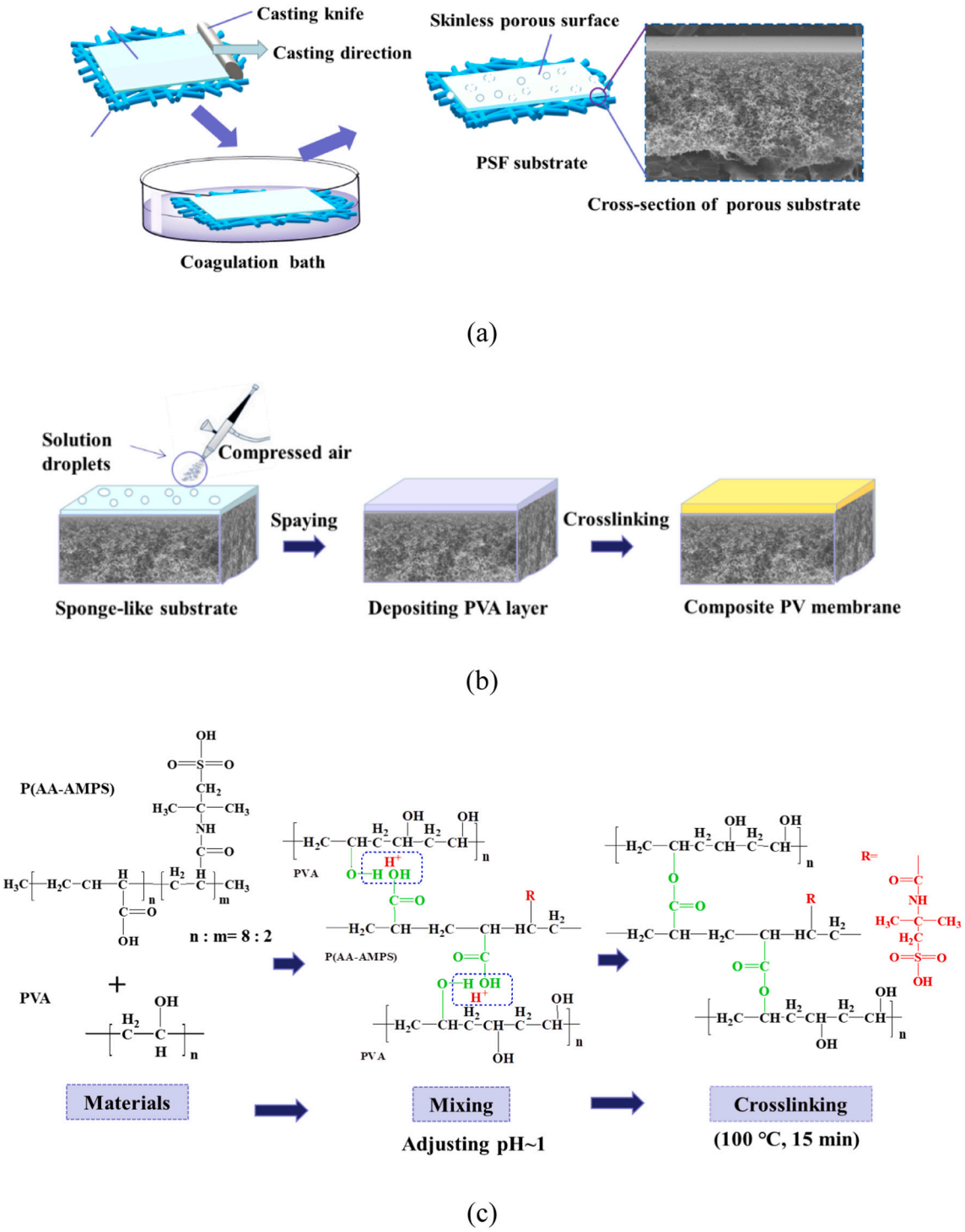

Fig. 1. Illustrations the preparation processes of (a) the PSF ultra-filtration membranes, (b) the spray-coating and (c) the post cross-linking.

operation cost and high-water production quality [7,8]. However, as a byproduct of SWRO, a great deal of concentrated brine is generated and then discharged directly to environment, jeopardizing the marine ecology system tremendously [9,10]. Therefore, this is an urgent requirement for treating brine solutions.

In recent years, using pervaporation (PV) membrane for desalination has attracted much attentions due to the appealing desalination performance to highly concentrated salt solutions, anti-fouling property and great improvement in water flux [11–13]. For example, by tuning the structures of the PSF substrates, Li et al. tuned series of PSF substrates based composite membranes for PV desalination, where the water fluxes were further increased to 60.8 kg/(m^2·h) at 70 °C for treating a 3.5 wt% NaCl solution [15]. To our best knowledge, the highest water flux of composite PV desalination membranes was reported by Xue et al. [16]. The water fluxes were dramatically increased by about 4 times (57.9 kg/(m^2·h) to 226 kg/(m^2·h) at 75 °C) when the support layers were changed from a chlorinated polyvinyl chloride (CPVC) ultra-filtration membrane prepared by NIPS to a porous electrospun polyacrylonitrile (PAN) nanofiber mat. All these results demonstrated that the membrane substrate played a crucial role in designing high water flux PV composite membranes. The ultrahigh water flux is largely benefited from the substrate structure that having a highly porous, inter-connected, and skinless cross-sectional morphology. However, the electrospinning requires fine regulation. Any fluctuation in temperature, air humidity, voltage may lead to significantly changes in fiber morphology and pore size of the fibrous mat [17]. More importantly, electrospinning is costly and time-consuming. Since the surface pore size of a fibrous mat is depended on the fiber diameter, slimmer fibers are preferred to obtain a fibrous mat with smaller surface pore sizes [18]. This requires a much-diluted spinning solution and prolongs the electrospinning process. Sometimes an intermediate layer is needed to reduce the surface pores of an electrospun substrate for coating a defect-free top layer [19]. Therefore, it is a big challenge to scale up composite PV membrane based on electrospinning technology. On the other hand, it is not trivial to develop an easily scaled-up method (i.e. NIPS technology) to prepare high-performance PV desalination membranes.

In this work, we aimed to develop a high property pervaporation (PV) desalination membrane using a NIPS substrate, where the key factor was to design a porous substrate structure with less gas transport resistance. Polysulfone (PSF) was selected as the base membrane material due to its low cost, easy processing and excellent physio-chemical stability [20]. Its hydrophilicity was improved by blended with certain amount of sulfonated polysulfone (SPSF). Effects of the organic additives including polyvinylpyrrolidone (PVP) and propionic acid (PA) [21,22] and the coagulant bath temperature on the membrane morphology [23] were studied. Consequently, a PSF membrane with a macro-void free and skin-less cross-sectional structure was fabricated successfully. After spray-coating a dense PVA layer, the composite PV membrane achieved a high water flux of 124.8 ± 3.2 kg/(m^2·h) with a salt rejection over 99.9% for treating a 3.5 wt% NaCl solution at 70 °C. When treating a 20 wt% NaCl solution at 70 °C, a high-water flux of 71.3 ± 1.8 kg/(m^2·h) was achieved. Moreover, attributing to the mechanical inter-lock structure at the interface of the PSF and PVA layers, the composite PV membranes were free of delamination during the relatively long operation period of 480 min.

In summary, we demonstrated that, for the first time, PV desalination membranes based on a substrate prepared by a NIPS process could have a water flux over 100 kg/(m^2·h) which was two times higher than other PV desalination membranes using the same NIPS PSF substrate [15,16,41–43]. This indicated that high performance PV desalination membranes could be prepared using conventional and already commercialized techniques.

Table 1
The PSF membrane ID, dope compositions and coagulation bath temperature.

Membranes ID	PSF (wt %)	SPSF (wt %)	PVP (wt %)	NMP (wt %)	PA (wt %)	Coagulation bath temperature (°C)
PA0-25	11.9	2.1	10	76	0	25
PA5-25	11.9	2.1	10	71	5	25
PA10-25	11.9	2.1	10	66	10	25
PA15-25	11.9	2.1	10	61	15	25
PA15-40	11.9	2.1	10	61	15	40
PA15-60	11.9	2.1	10	61	15	60

2. Experimental

2.1. Materials

Polysulfone (Udel P1700) was supplied by Solvay S.A Co., Ltd. Sulfonated polysulfone (SPSF) (sulfonation degree: 30%) was obtained from Shandong Jinlan Polymer Co., Ltd. *N*-methyl-2-pyrrolidone (NMP, purity ≥99.0%) and 98 wt% sulfuric acid (H_2SO_4) were bought from Tianjin Da Mao Chemical Reagent Factory (China). Propanoic acid (PA, M_w: 74 g/mol) was supplied by Tianjin Fuchen Chemical Reagent Factory (China). Polyvinylpyrrolidone (PVP, K-30, M_n: 44,000–54,000) was got from Gongbike New Material Technology Co., Ltd. Polyethylene terephthalate (PET) non-woven fabric was supplied from Shanghai Pole Technology Co., Ltd. Polyvinyl alcohol (PVA, M_w: 104,000 g/mol, hydrolysis degree: 99.4%) and sodium chloride (NaCl, purity ≥99.9%) were purchased from Sinopharm Chemical Reagent Co., Ltd. (China). Poly acrylic acid co-2-acrylamido-2-methyl propane sulfonic acid (P(AA-AMPS), M_w: 2000–5000 g/mol) in a 30 wt% water solution was obtained from Shandong Usolf Chemical Technology Co., Ltd. Bovine serum albumin (BSA, M_w: 67,000 g/mol) was supplied by Sigma-Aldrich Co., Ltd. A lab-equipped Millipore ultrapure water system was adopted to produce deionized (DI) water.

2.2. PVA/PSF composite PV membrane fabrication

2.2.1. Preparation of the PVA free-standing films

Firstly, 6 g of PVA was dissolved in 94 mL of DI water, stirred at 90 °C for 2 h to get a homogenous PVA solution. Secondly, the solution consisting of PVA and P(AA-AMPS) at a weight ratio of 7 to 3 and a pH value of 1 adjusted by H_2SO_4 was prepared. Next, the mixed solution was degassed for 24 h and then casted on a PTFE substrate. Then, dense free-standing PVA films were formed after evaporating of water at room temperature for 48 h. By controlling the amount of casting solution, the PVA film thickness was controlled at 70 ± 10 μm. At last, the PVA dense films were crosslinked in a muffle furnace (100 °C, 15 min, air atmosphere).

2.2.2. Preparation the PSF ultra-filtration membranes

The procedure of the preparation of the PSF membranes is given in Fig. 1a [24]. Table 1 lists the manufacture parameters and membrane IDs. In a typical process, a polymer dope consisting of PSF, SPSF, PVP, NMP and PA was cast onto a PET non-woven fabric and then transferred into a water bath immediately to induce phase inversion. The water bath was refreshed once a day for three days to remove the residual solvent and additives completely. After that, water in the membrane was exchanged with methanol followed by n-hexane and dried at an ambient condition, as reported in ref. [25].

2.2.3. The spray-coating and post cross-linking processes

Using a similar method of our previous work [26], the composite membranes were prepared by spraying-coating as illustrated in Fig. 1b. Specifically, a 0.5 wt% aqueous solution consisting of PVA and P(AA-AMPS) at a weight ratio of 7 to 3 and a pH value of 1 adjusted by H_2SO_4 was sprayed onto a PSF membrane using an air-brush. The

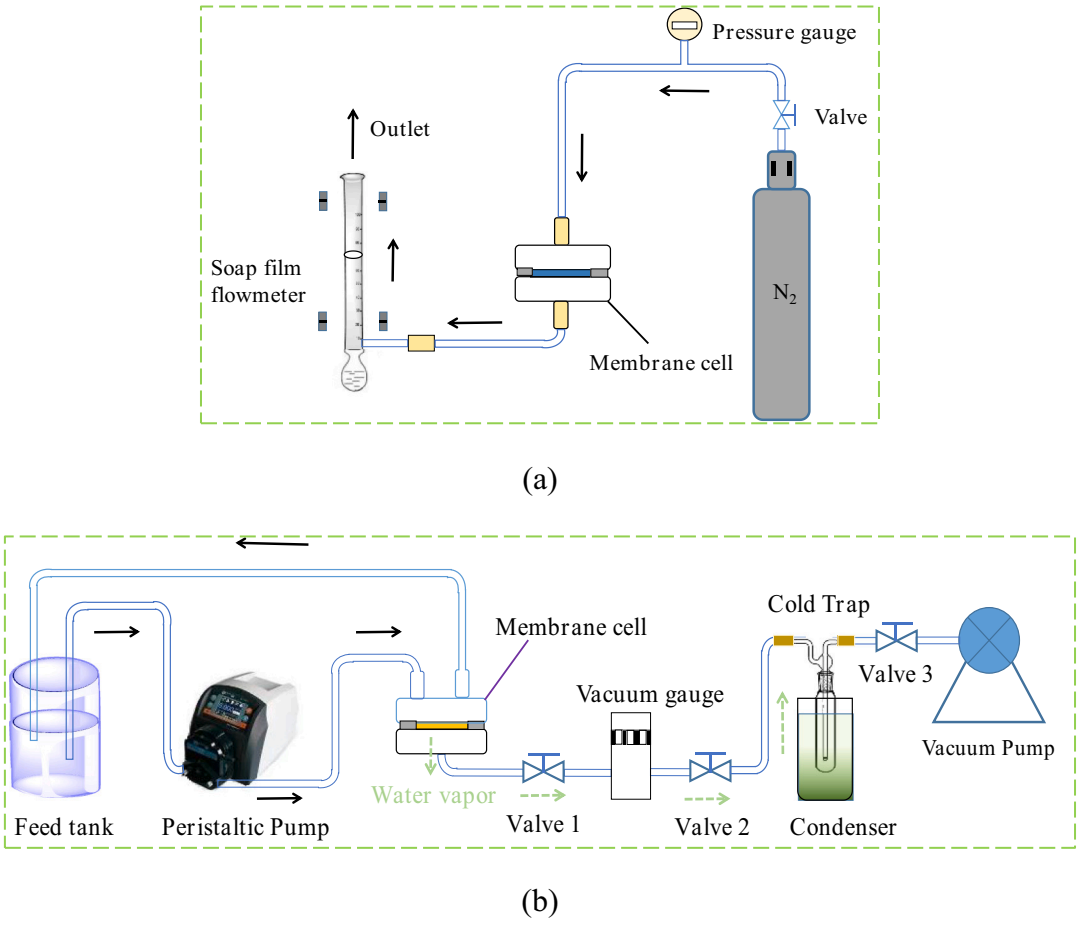

Fig. 2. Schematic diagrams of the processes of (a) the gas resistance measurement for the substrates and (b) the PV measurement.

distance between the nozzle and the membrane surface was 15 cm and the air pressure of the air-brush was maintained at 2–3 bar. Thickness of the coating layer was adjusted by controlling the spraying volumes.

After coating, the composite membranes were heated at 100 °C for 15 min to cross-link the PVA layer as shown in Fig. 1c. The composite membrane was cooled in ambient temperature for 4 h then the residual H_2SO_4, unreacted PVA and cross-linker were washed off with DI water. At last, the composite membranes were dried in air before test.

2.3. Characterizations of the membrane substrates

2.3.1. Determination of the membrane morphologies

A scanning electron microscope (SEM) (HITACHI S-7800 Japan) was used to monitor the cross-section and surface morphology of the membranes. The average pore size and porosity at surface of the PSF membranes were estimated based on the SEM image using an image J software as introduced in ref. [27]. Thicknesses of the PVA layers were determined from the SEM image by a Nano Measurer software. All the samples were fractured in liquid nitrogen to obtain a smooth cross section and then sputter-coated with gold before testing.

2.3.2. Gas permeation tests

A lab-made gas permeation cell was used to estimate the gas transport resistance of the PSF membranes as shown in Fig. 2a. A detailed introduction of the equipment could be found in Ref. [28]. Generally, the gas permeation cell would measure a series of N_2 flux at elevated trans-membrane pressures. Then, the relation between the trans-membrane pressure and N_2 flux could be correlated using Eq. (1):

$$Q = \frac{V}{A \times T} \tag{1}$$

where Q was the gas flux of N_2 (L/(m^2·h)); V was the volume of the N_2 (L); A was the effective membrane area (m^2); and T is the data collection time (h). By plot Q vs T, a linear curve could be obtained and the slope of the curve was used to calculate the gas transport resistance of the membrane.

2.4. Swelling degree

Dried PVA/P(AA-AMPS) self-standing films and the PSF substrates were weighted to get their dry weights and recorded as m_d(g). Then they were immersed in DI water at room temperature for 24 h, respectively, to reach sorption equilibrium. After wiping off water drops on the sample surface, the wet weight was measured and recorded as m_s(g). The water swelling degree (SD, %) was calculated using Eq. (2) [29]:

$$SD = \frac{m_s - m_d}{m_d} \times 100\% \tag{2}$$

For each sample, the measurement was repeated for 3 times to get an average data.

2.5. Characterizations of the composite membrane

2.5.1. Determination of the interface bonding force

To calculate the interface bonding force between the S-PVA dense selective layers and PSF substrate, a stretching method was adopted using a dynamic mechanical analyzer (DMA) (Q800, TA, USA) (Fig. 9S). A stretching force was applied perpendicular to composite membranes

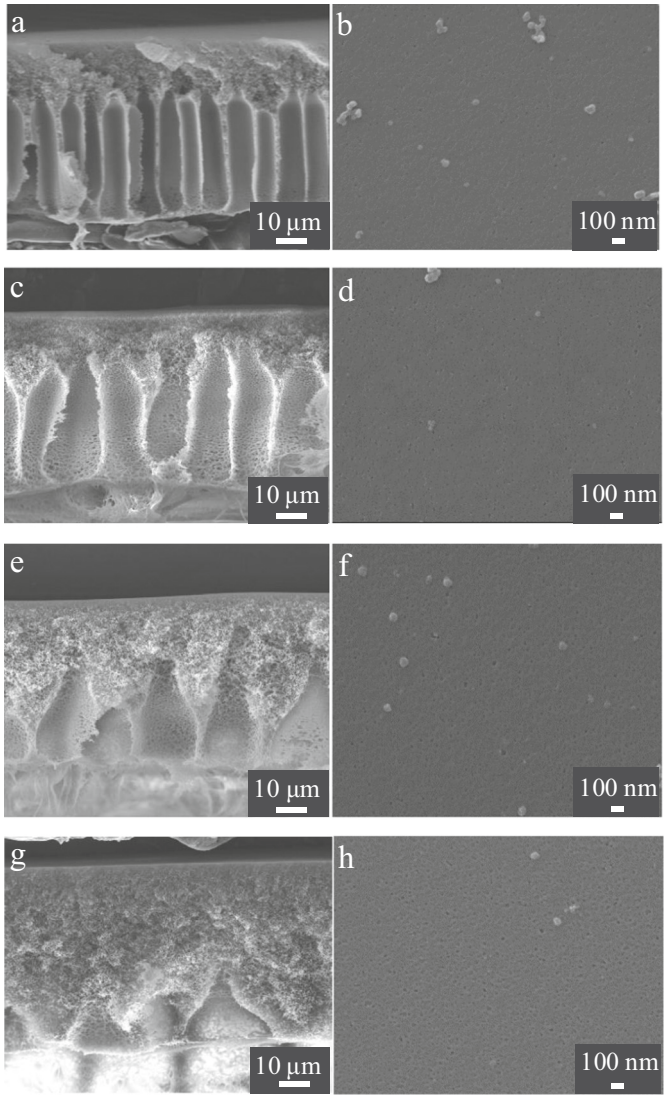

Fig. 3. SEM images surface and cross-sectional morphology of PSF membranes with PA concentrations of 0% (a, b), 5% (c, d), 10% (e, f) and 15% (g, h).

until the PSF substrate separated from the S-PVA layer. The tensile ~stress curve was recorded as the adhesive strength in the control force mode at a rate of 0.2 N/min until they were torn apart. Before the test, the front and back surfaces of the composite membrane were affixed between two glass plates using an adhesive tape, clamped by a DMA fixture.

2.5.2. PV desalination properties

The PV desalination properties were evaluated using a lab-equipped PV set-up as shown in Fig. 2b. A detailed description of the equipment and the testing protocol could be found in ref. [16]. In this work, saline solutions with a NaCl concentration of 0–20 wt% were used as feeds. The feed solution was circulated at membrane feed side with a flow rate of 0.1 m/s. Membrane permeate side was vacuumed at 100 Pa. the permeated water vapor was collected using a liquid nitrogen cold trap. During the PV test, the permeated water vapor was collected in 15 min to calculate the permeate flux using Eq. (3). At each testing condition, at least 3 independent tests were carried out, the average was reported.

$$J_w = \frac{M}{A \times T} \tag{3}$$

where J_w was the permeate flux (kg/(m^2·h)); A was the effective membrane area (m^2), which was 3.28 cm^2; and T was the operation period (h). The salt concentrations of the feed and permeate samples were analyzed by an electrical conductivity meter (DDSJ-308F, Lei chi, China). The salt rejection (R) was determined using Eq. (4):

$$R = \left(\frac{C_f - C_P}{C_f}\right) \times 100\% \tag{4}$$

where C_p(wt%) was the permeate salt concentration; C_f(wt%) was the feed salt concentration.

3. Results and discussion

3.1. Preparation of the PSF membranes with macro-void free structure

In a typical NIPs process, a polymer dope may undergo two types of phase inversion processes: nucleation and growth (NG) and spinodal decomposition (SD). When a phase separation starts at the meta-stable region of a triangle phase diagram for a polymer-solvent-nonsolvent system, NG takes place and it usually leads to the formation of macro-voids in a membrane. On the other hand, when a phase inversion happens inside the spinodal region, SD occurs and leads to the formation of a membrane with a bi-continuous structure. Since the spinodal region is inside the binodal curve of a phase diagram, a precipitation path of a polymer dope must pass through the meta-stable region first and then enters the spinodal region to induce the SD phase inversion. Because we want to prepare a membrane with a macro-void free structure, the NG phase inversion shall be inhibited.

As suggested by Su et al. [30], increasing viscosity of a polymer dope can delay the phase inversion process so that the phase separation can be postponed till the dope composition falls into the spinodal region. Initial attempt was to add PVP into the PSF/SPSF dope to increase its viscosity. It was reported that PVP suppressed the formation of macro-voids [31]. Fig. 3a shows that the PSF/SPSF/PVP membrane exhibits a typical asymmetric structure with a relatively dense top skin layer and a sub-layer having a sponge-like bi-continuous structure that gradually turns into finger-like macro-voids. It can be seen the dense top layer and the sponge-like upper half region of the membrane are formed by SD, while the lower part of the membrane is formed by NG mechanism. Due to the high viscosity of the polymer dope, the relaxation time of the polymer chain is long that suppresses the nucleation of polymer rich and lean phases. Meanwhile, the solvent/non-solvent continuously exchanges and the dope composition falls into the spinodal region. Subsequently, SD takes place and forms the bi-continues sponge-like structure on the upper part of the membrane. Once the upper part of the dope precipitates, the solvent/non-solvent exchange rate decreases significantly. The polymer dope at the lower part has more time to stay in the meta-stable region of the phase diagram. Hence, there is sufficiently time for the nuclei to form and finally grow into macro-voids at the lower part of the membrane.

To solve the contradiction between macro-void free structure and low membrane flux, PA is added to the dope solution as a second non-solvent additive. PA has a capable of forming a Lewis acid–base complex with NMP [32]. The PA: NMP complex reduces the solvent power of NMP and promotes polymer chain aggregation [33]. These effects further increase the dope viscosity and retard the formation of macro-voids. As shown in Fig. S1, the PSF solution viscosity increases exponentially with the PA concentration [34]. More importantly, as a small organic molecule, PA diffuses into the polymer lean phases easier than the high molecular weight PVP. Consequently, solvent of the polymer rich phase will diffuse into the polymer lean phases. This causes the increment of the polymer concentration in the polymer rich phase and the formation of polymeric micelles that leads to the formation of bigger pores on membrane surface [35]. As illustrated in Fig. 3c, e, and g, when the PA concentration increases from 5 to 15 wt%, the surface porosity and average surface pore diameters gradually increases from 4.4% to

Table 2
The average surface pore sizes, surface porosities, overall membrane porosities and water flux of the PSF substrates.

Membrane ID	Surface pore size (nm)	Surface porosity (%)	Overall porosity (%)	Water flux (kg/(m^2·h·bar))	Coagulation bath temperature (°C)
PA0-25	8.1	4.4	52.8	453.3 ± 2.4	25
PA5-25	9.0	5.5	53.0	471.1 ± 9.1	25
PA10-25	9.3	7.5	54.3	504.2 ± 14.1	25
PA15-25	10.3	8.9	55.0	654.3 ± 18.2	25
PA15-40	15.9	11.3	55.2	897.2 ± 30.9	40
PA15-60	25.2	14.9	56.5	1014.8 ± 27.6	60

8.9% and 8.1 to 10.3 nm, respectively. Moreover, the finger-like macro-voids gradually move away from the surface of the PSF membrane. Hence, the incorporation of PA retards the formation of macro-voids, at the same time, increases surface pore sizes of the membrane. Therefore, the pure water fluxes of the PSF membranes increase from 453.3 ± 2.4 kg/(m^2·h·bar) to 654.3 ± 18.2 kg/(m^2·h·bar), as listed in Table 2.

3.2. Optimizing the PSF substrates for skin less layer structure

Nevertheless, a thick skin layer still exists in all the PSF membranes. Not only that thick layer significantly increases the transport resistance [23], but also limits the solvent/non-solvent exchange rate and thus eventually causes the formation of macro-voids on the bottom of the membrane. To get rid of the skin layer, temperature of the coagulant bath is increased. Typically, the solvent/non-solvent exchange rate will be greatly enhanced at a high temperature. This facilitates the instantaneous phase inversion that results in a membrane structure with big pores [36]. As shown in Fig. 4f, and i, macro-void free cross-sections of the membranes prepared at 40 °C and 60 °C are obtained. Most important, all the macro-void free membranes have a loosely packed skinless structure (Fig. 4e, h) and the surface average pore diameters (Fig. 4d, g) and porosity further increase from 10.3 nm to 25.2 nm and 8.9% to 14.9%, respectively, as listed in Table 2. Therefore, the pure water fluxes of the PSF membranes (PA15-60) increase from 654.3 ± 18.2 kg/(m^2·h·bar) to 1014.8 ± 27.6 kg/(m^2·h·bar) benefiting from the enlarged surface pore sizes and skinless structures.

3.3. Effects of the substrate structure on the gas transport resistance

In a PV desalination process, the water molecules desorb from the backside of the dense selective layer of PV composite membrane and then permeate through the porous substrate in a gas state [37,38]. Therefore, determining the gas transport property of the substrate can better understand the transport resistance of the support layer of the composite membranes. Since it is difficult to maintain a constant water vapor pressure, we test the N_2 gas flux of the membranes under different pressures. Fig. 5a shows that all the N_2 fluxes increase linearly with the trans-membrane pressures. And the gas flux of the PSF membranes prepared at 25 °C using a polymer dope with 15 wt% PA is higher than those of the membranes fabricated with polymer dopes having less amount of PA (0, 5, and 10 wt%). Because the gas flux was sensitive to the membrane surface pores radius and porosity according to the viscous flow model (Eq. (S3)), the higher gas flux of PA 15 match its larger surface pore sizes and surface porosities, as listed in Table 2. Nevertheless, significant transport resistance still exists on its composite PV

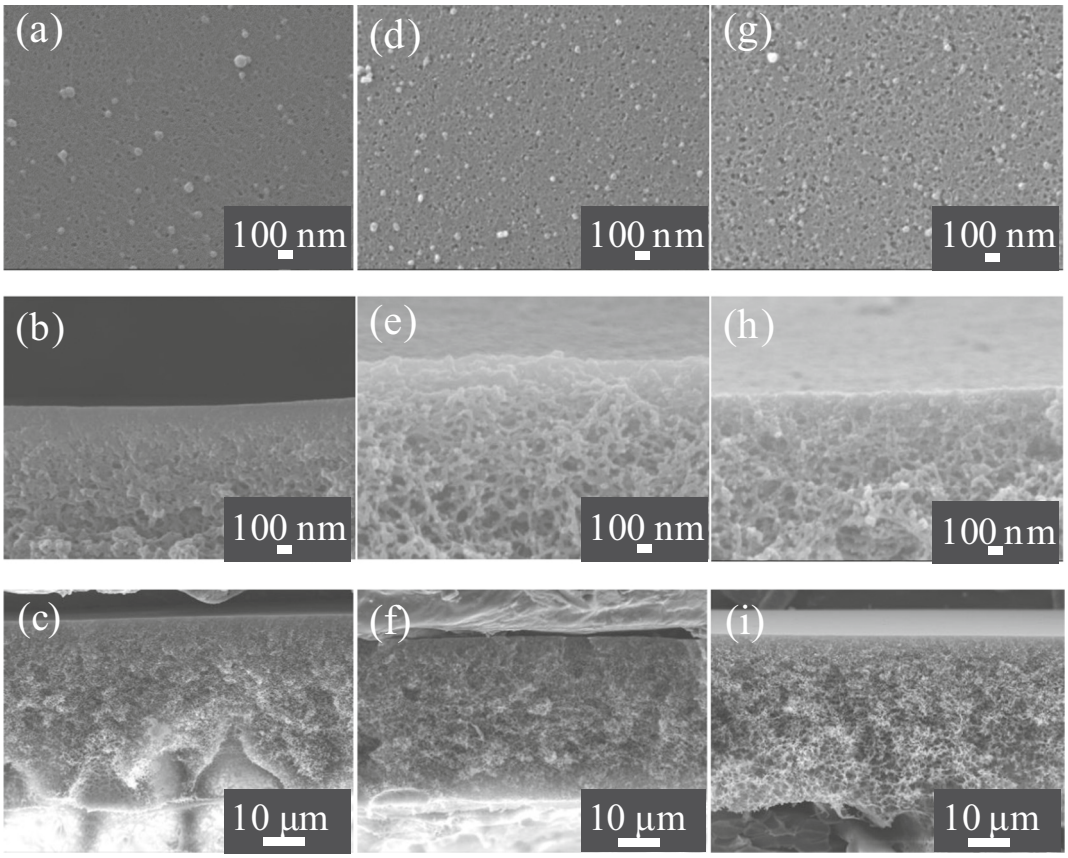

Fig. 4. SEM images of surface, top skin layer and cross-section of PSF/PA membranes at different coagulation bath temperature: (a, b, c) 25 °C, (d, e, f) 40 °C and (g, h, i) 60 °C.

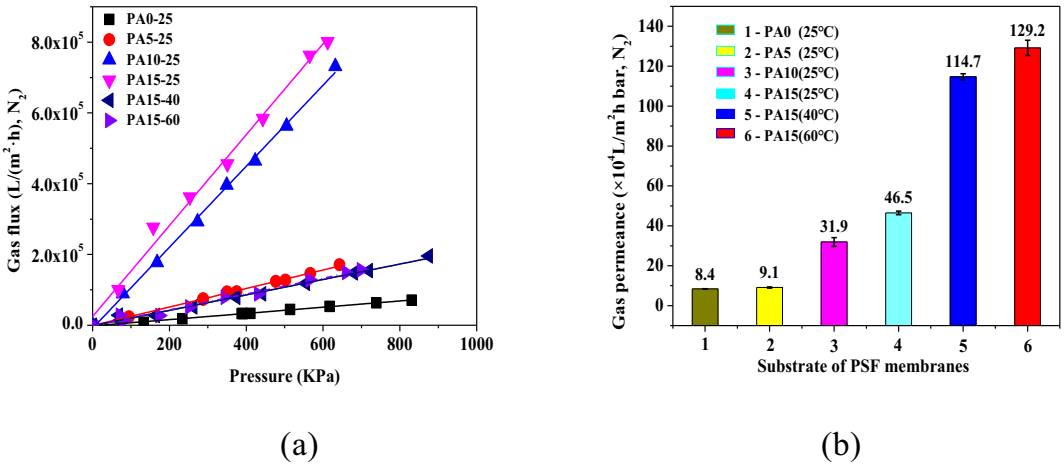

Fig. 5. (a) The N_2 fluxes at elevated pressures of all PSF membranes (kPa) and (b) the gas permeance for all substrate of PSF membrane.

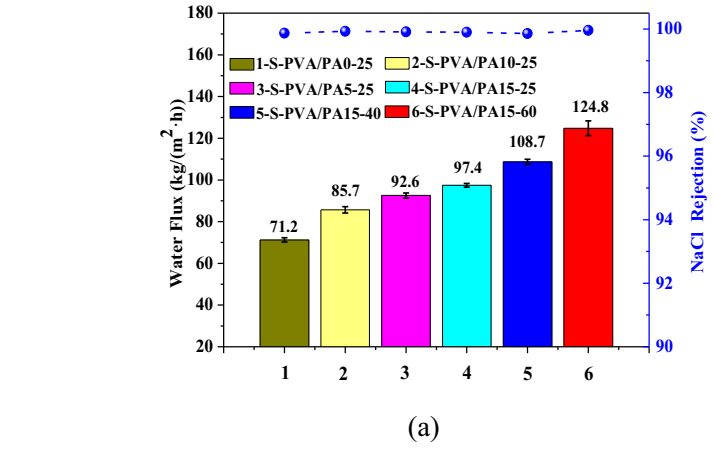

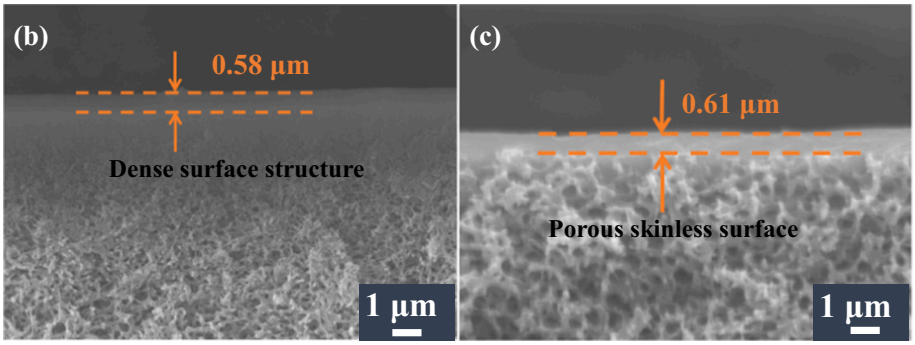

Fig. 6. (a) The water fluxes and salt rejections of the composite PV membranes using a 3.5 wt% NaCl solution as feed at 70 °C; SEM images of the outer-most regions of the membrane cross-sections: (b) and (c) refer to the PSF substrates prepared in water coagulants of 25 °C and 60 °C.

membrane for a thick skin layer of the PSF membranes (PA15-25, Fig. 4b). By simply increasing the coagulant temperature to 60 °C, the instantaneous phase inversion process was accelerated, and the substrate became more porous (surface pore sizes and porosity were greatly enhanced to 25.2 nm and 14.9%). As a result, the PA15-60 membrane achieved a highest gas performance (129.2 × 10^3 L/(m^2·h·bar)), which is 4.8 times higher than that of PA15-25 membrane (26.9 × 10^3 L/(m^2·h·bar)). Therefore, the PA15-60 based composite PV membranes shall exhibit the highest water flux due to the lowest resistance of the substrate [39].

3.4. Pervaporation desalination properties

Desalination properties of the PVA/PSF composite PV membranes are evaluated using an aqueous solution comprising 3.5 wt% NaCl at 70 °C as feed. Fig. 6a reveals that all membranes have a salt rejection greater than 99.9%. This indicates that the PVA selective layer is defect-free. The water fluxes gradually increase from 71.2 ± 1.0 kg/(m^2·h), 85.7 ± 1.4 kg/(m^2·h) to 97.4 ± 0.7 kg/(m^2·h), as the concentrations of the PA additives in the PSF dope solutions increase from 0, 5, to 15 wt%. Note that, the thicknesses of the S-PVA layers among all composite membranes are similar (~0.6 μm, Fig. 6b, c). Therefore, the improvement in water flux must be due to the decrements in the gas transport

Table 3
Swelling degree of the PVA, cross-linked PVA film and PSF substrates.

Sample	Density (g/cm^2)	Thickness (μm)	Original mole ratio of (-OH):(-COOH)	Swelling degree (%)
PVA film	1.28	73.0 ± 4.7	–	Dissolve
Cross-linked PVA film	1.30	65.3 ± 8.2	11.3:1	193.4 ± 55.6
PSF membrane	1.24	61.3 ± 5.5	–	54.5 ± 1.4

resistance of the PSF substrates. This trend becomes more clearer as the substrate membrane coagulation temperatures increase from 25 °C to 60 °C, where the PV water flux further increases by 1.8 times to 124.8 ± 3.2 kg/(m^2·h). Based on the results listed in Table 2 and the membrane morphologies shown in Fig. 6, the high coagulant temperature and PA content in the polymer dope eventually lead to the formation of a PSF substrate with a skinless, highly porous and inter-connected cross-sectional structure (Fig. 6c). As a result, the gas transport resistance of the PSF substrate is greatly reduced and consequently promotes the water flux of the composite PV membrane.

3.5. The resistance to delamination and long-term operational stabilities

Once delamination between the coating layer and the substrate occurs, the separation performance of a composite membrane will deteriorate. To ensure a stable separation property, a strong adhesive force to the coating layer is preferred. In this study, the sulfonic acid groups in the S-PVA absorb a large amount of water. The water swelling degree of the cross-linked S-PVA is 193.4 ± 56.5%, which is much higher than that of the PSF substrate (54.5 ± 1.4% as listed in Table 3). The big differences in their water swelling ratios lead to a serious delamination problem. As shown in Fig. S6 in the supporting information, some wrinkles are observed on surface of the water-swelled S-PVA/PA0-25 membrane. By contrast, surface of the S-PVA/PA15-60 membrane is smooth indicating a better compatibility between the two layers. Similarly, after drying, the wrinkles appear more clearly on the surfaces of the composite membranes on top of the PA0-25, PA5-25, PA10-25, and PA15-25 substrates, but not on those of the PA15-40 and PA15-60 substrates (Fig. 7). We hypothesize that the relatively smooth surfaces of the first four substrates provide limited contact surface to the S-PVA coating layer and cannot prevent the delamination of the swelled S-PVA

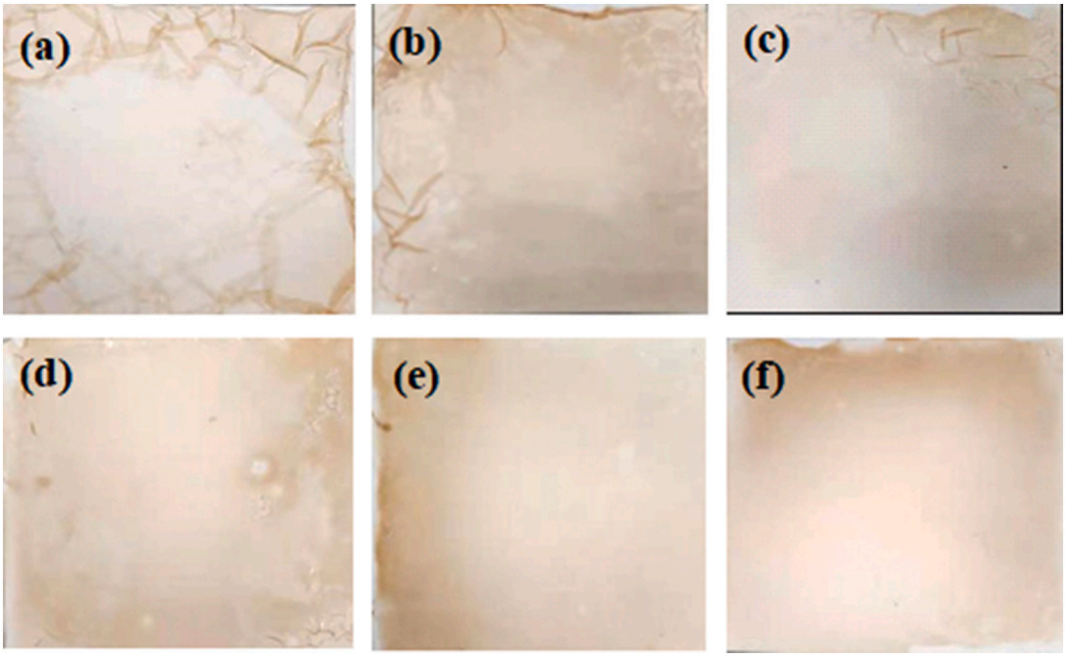

Fig. 7. Surface images of dried PVA films falls from the PSF substrates of composite membranes: (a) S-PVA/PA0-25, (b) S-PVA/PA5-25, (c) S-PVA/PA10-25, (d) S-PVA/PA15-25, (e) S-PVA/PA15-40 and (f) S-PVA/PA15-60.

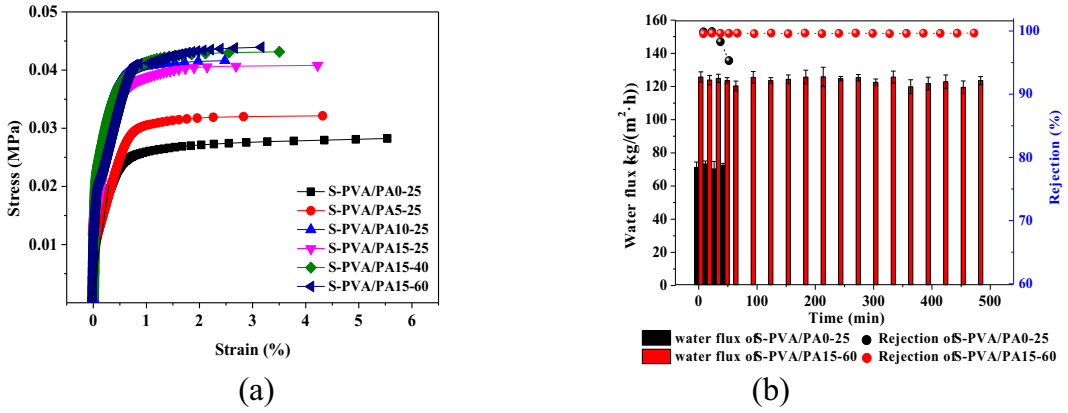

Fig. 8. (a) Stress and strain relationship of the composite membrane and (b) the long-term stability PV tests of the S-PVA/PA0-25 and S-PVA/PA15-60 membrane.

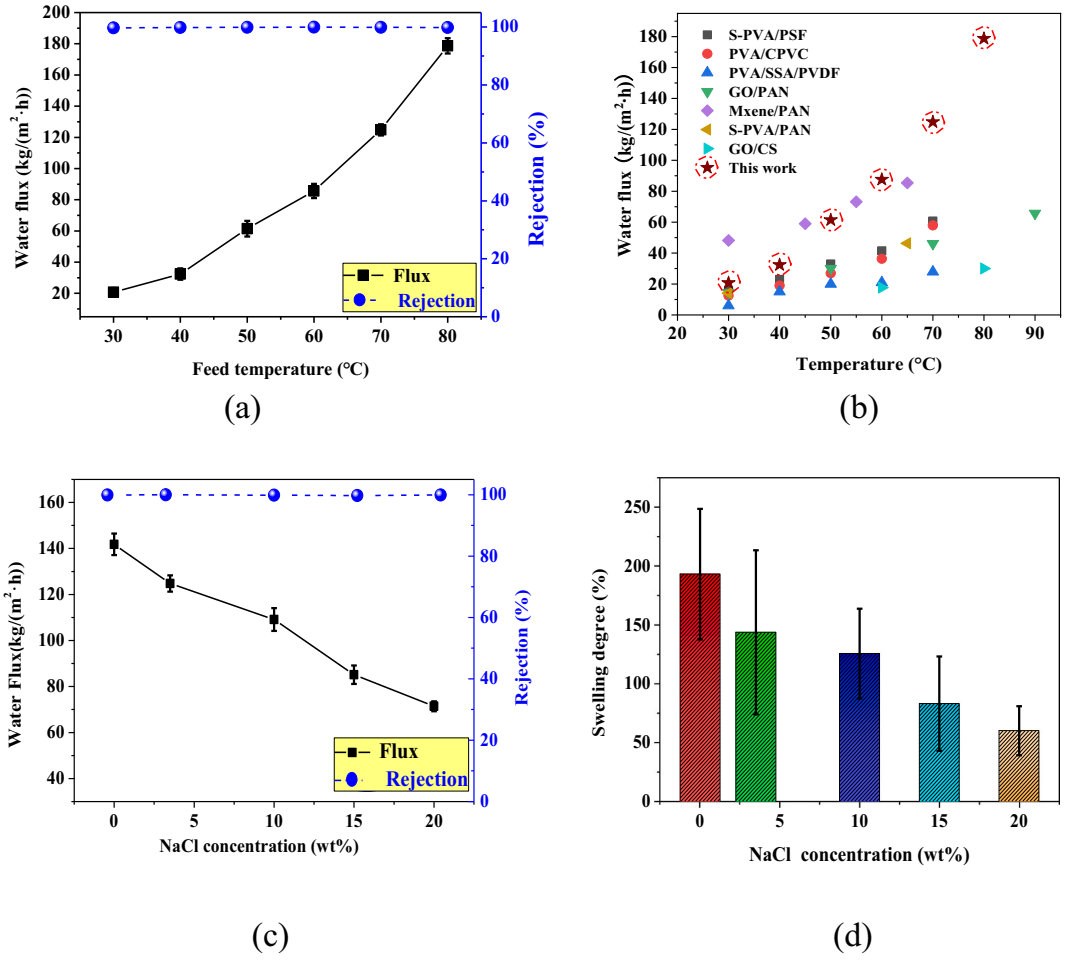

Fig. 9. (a) Desalination performance of the S-PVA/PA15-60 at varied feed temperature; (b) comparison our membranes performance with the reported membranes; (c) desalination performance of the S-PVA/PA15-60 at varied feed NaCl concentration at 70 °C and (d) the swelling degree of the self-supporting PVA films at NaCl concentration from 0 wt% ~ 20 wt%.

layer. In contrast, the PA15-40 and PA15-60 substrates have a skinless structure that offers much rougher surface morphologies with bigger surface pores (AFM images in Fig. S7). Hence, the intrusion of the S-PVA coating solution during the spray-coating process and the larger contact area to the coating layer successfully prevent the formation of wrinkles of the water-swelled S-PVA layer as shown in Fig. 7e and f.

The bonding forces between the two layers of the composite membranes are determined using a method (illustrated in Fig. S9), as introduced in ref. [26]. Fig. 8a shows the stress-strain diagram of all six composite membranes. The highest stress of each diagram is obtained as the delamination of the composite membrane happens. It can be seen the delamination stresses of the S-PVA/PA15-60 and S-PVA/PA15-40 membranes are about 0.044 MPa, 1.6 times higher than that of the S-PVA/PA0-25 membrane. The higher adhesive forces of the S-PVA/PA15-40 and S-PVA/PA15-60 membranes agree well with their good resistance to delamination (Fig. 7). Therefore, no PSF membranes were torn off from the PVA films for the S-PVA/PA15-60 benefiting for its good interface adhesion, while some parts of PSF membrane (white) of S-PVA/PA0-25 membrane were peeled off at a low stretching force, as illustrated in Fig. S10 in the supporting information. The better stability of the S-PVA/PA15-60 composite membrane is also proved by the long-term PV desalination tests. Fig. 8b presents that the water fluxes and salt rejections of the S-PVA/PA0-25 composite membrane decreases in less than 45 min, while that of the S-PVA/PA15-60 membrane is stable during the entire 480 min testing period.

3.6. Effects of temperature and salt concentration on the desalination properties

Pervaporation desalination performance of the S-PVA/PA15-60 membranes at different temperatures was measured using a 3.5 wt% NaCl solution as feed. Fig. 9a illustrates that the water fluxes increase from 20.8 ± 1.3 kg/(m^2·h) to 178.7 ± 3.9 kg/(m^2·h) when the feed temperature increases from 30 °C to 80 °C. This can be explained by well-known Arrhenius relation between temperature and membrane flux. The partial pressure of water vapor at the feed side increases exponentially with the increasing feed temperature, and thus enhances the water driving force of transferring composite membrane [40]. As shown in Fig. 9b, our membrane achieves a highest level of water flux that overshadows all the composite PV desalination membranes using substrates prepared by the NIPS method [15,16,41–43].

One of the application scenarios for the PV membranes is the highly concentrated brine solutions. We have tested the desalination properties of the S-PVA/PA15-60 membrane to concentrated brine water. As shown in Fig. 9c, the water flux decreases drastically from 124.8 ± 3.2 kg/(m^2·h) to 71.3 ± 1.8 kg/(m^2·h) at 70 °C, as the content of NaCl increases from 3.5 wt% to 20 wt%. The decrements can be mainly attributed to the de-swelling effect of the concentrated brines [43]. Fig. 9d shows that the water swelling degree of the S-PVA polymer drastically decreases from 193.4 ± 55.6% to 60.5 ± 21.0% by increasing the salt concentration. As a result, the driving force for water transport decreases. The water concentration in the S-PVA membrane is reduced

Table 4
The water concentrations in the S-PVA polymer, theoretical water flux, and partial pressure of water vapors.

NaCl content (wt%)	Water content in the swelling membrane ($\times 10^4$ mol/m^3)	Experimental water flux (kg/(m^2·h))	Theoretical water flux (kg/(m^2·h))	The partial water vapor pressure (kPa)
0	4.0	142.0	142.0	31.16
3.5	3.6	124.8	127.8	31.03
10	3.4	108.4	120.7	30.82
15	2.9	85.1	103.0	30.12
20	2.4	71.3	85.2	28.96

from 4.0 × 10^4 mol/m^3 to 2.4 × 10^4 mol/m^3, as listed in Table 4. Moreover, we have calculated the theoretical water flux based on the de-swelling effect and found that the estimated water fluxes were higher than that of experimentally determined water fluxes. The severer concentration polarization effect [44–46] may cause the inconsistency as reported in ref. [19]. Despite of the de-swelling and concentration polarization effects of the high concentration brines, the membrane could also achieve a high performance of 71.3 ± 1.8 kg/(m^2·h) at 70 °C. In summary, the easy-to-scale-up fabrication of the high-performance composite PV membranes suggests a great potential for industrialized applications.

4. Conclusion

In this work, high performance of PVA/PSF pervaporation desalination membrane was fabricated by spay-coating an ultra-thin PVA layer (~0.6 μm) onto a PSF ultrafiltration membrane prepared by a NIPs method. By tailoring the composition of the PSF dope using PVP and PA non-solvent additives and the coagulation bath temperature, the targeted PSF membranes with skinless surface, macro-void free bi-continuous cross-sectional morphology were obtained, which had very low gas transport resistance. Water flux of PVA/PSF composite membrane reached to 124.8 ± 3.2 kg/(m^2·h) for separating a 3.5 wt% NaCl solution at 70 °C, which was the highest reported data among all the PV composite membranes based on NIPS substrates. Also, a high-water flux of 71.3 ± 1.8 kg/(m^2·h) could be achieved for treating high concentrated solution of 20 wt% at 70 °C. The composite membranes were stable during a 480 min PV desalination test because the enhanced the adhesive strength between interface of the PVA layer and the PSF substrate that had a skinless and rough surface. The easy-to-scale-up fabrication method, as well as the high performance, indicates a great potential of PVA/PSF composite PV membranes for desalination.

CRediT authorship contribution statement

There are no conflicts of interest with other researchers or groups.

Declaration of competing interest

There are no conflicts of interest with other researchers or groups.

Acknowledgement

This research is funded by National Key Research and Development Program of China (2021YFC2101201-3).

Appendix A. Supplementary data

Supplementary data to this article can be found online at https://doi.org/10.1016/j.desal.2021.115496.

References

[1] M. Elimelech, W. Phillip, A the future of seawater desalination: energy, technology, and the environment, Science 333 (2011) 712–717.
[2] N. Ghaffour, T. Missimer, G.L.M. Amy, Technical review and evaluation of the economics of water desalination: current and future challenges for better water supply sustainability, Desalination 309 (2013) 197–207.
[3] C.N. Kim, T. Kyaw, J.O. Seung, A. Li, W.S. Muhammad, B. Azhar, Recent developments in thermally-driven seawater desalination: energy efficiency improvement by hybridization of the MED and AD cycles, Desalination 356 (2015) 255–270.
[4] E. Drioli, A. Ali, F. Macedonio, Membrane distillation: recent developments and perspectives, Desalination 356 (2015) 56–84.
[5] M.A. Shannon, P.W. Bohn, M. Elimelech, J.G. Georgiadis, B.J. Marinas, A. M. Mayes, Science and technology for water purification in the coming decades, Nature 452 (2008) 301–310.
[6] M.Q.E. Jones, T.H. van Vliet Michelle, V. Smakhtin, S. Kang, The state of desalination and brine production: a global outlook, Sci. Total Environ. 657 (2019) 1343–1356.
[7] E. Drioli, A.I. Stankiewicz, F. Macedonio, Membrane engineering in process intensification-an overview, J. Membr. Sci. 380 (2011) 1–8.
[8] J. Kim, S. Hong, A novel single-pass reverse osmosis configuration for high-purity water production and low energy consumption in seawater desalination, Desalination 429 (2018) 142–154.
[9] T. Tong, M. Elimelech, The global rise of zero liquid discharge for wastewater management: drivers, technologies, and future directions, Environ. Sci. Technol. 50 (2016) 6846–6855.
[10] Q.Z. Wang, N. Li, B. Bolto, M. Hoang, Z.l. Xie, Desalination by pervaporation: a review, Desalination 387 (2016) 46–60.
[11] P. Swenson, B. Tanchuk, A. Gupta, W. An, S.M. Kuznicki, Pervaporative desalination of water using natural zeolite membranes, Desalination 285 (2012) 68–72.
[12] W. Kaminski, J. Marszalek, E. Tomczak, Water desalination by pervaporation-comparison of energy consumption, Desalination 433 (2018) 89–93.
[13] X. Chen, Y.B. Zhu, H. Yu, J.Z. Liu, C.D. Easton, Z. Wang, Y. Hu, Z. Xie, X. Zhang, D. Li, H. Wang, H.A. Wu, Ultrafast water evaporation through graphene membranes with subnanometer pores for desalination, J. Membr. Sci. 621 (2020), 118934.
[15] Q. Li, B. Cao, P. Li, Fabrication of high performance PV membrane by optimizing the support layer structure, Ind. Eng. Chem. Res. 57 (2018) 11178–11185.
[16] Y.L. Xue, J. Huang, C.H. Lau, B. Cao, P. Li, Tailoring the molecular structure of crosslinked polymers for pervaporation desalination, Nat. Commun. 1461 (2020).
[17] J.M. Deitzel, J. Kleinmeyer, D. Harris, N.C.B. Tan, The effect of processing variables on the morphology of electrospun nanofibers and textiles, Polymer 42 (2001) 261–272.
[18] H.Y. Ma, C. Burger, B.S. Hsiao, B. Chu, Fabrication and characterization of cellulose nanofiber based thin-film nanofibrous composite membranes, J. Membr. Sci. 454 (2014) 272–282.
[19] J.Q. Meng, P.B. Zhao, B. Cao, C.H. Lau, Y.L. Xue, R. Zhang, B. Cao, P. Li, Fabricating thin-film composite membranes for pervaporation desalination via photo-crosslinking, Desalination 512 (2021), 115128.
[20] Q.Z. Zheng, P. Wang, Y.N. Yang, Rheological and thermodynamic variation in polysulfone solution by PEG introduction and its effect on kinetics of membrane formation via phase-inversion process, J. Membr. Sci. 279 (2006) 230–237.
[21] B. Chakrabarty, A.K. Ghoshal, M.K. Purkait, Preparation, characterization and performance studies of polysulfone membranes using PVP as an additive, J. Membr. Sci. 315 (2008) 36–47.
[22] M.J. Han, Effect of propionic acid in the casting solution on the characteristics of phase inversion polysulfone membranes, Desalination 121 (1999) 31–39.
[23] D.J. Qin, R. Zhang, B. Cao, P. Li, Fabrication of high-performance composite membranes based on hierarchically structured electrospun nanofiber substrates for pervaporation desalination, J. Membr. Sci. 638 (2021), 119672.
[24] L. Zheng, J. Wang, D. Yu, Y. Zhang, Y. Wei, Preparation of PVDF-CTFE hydrophobic membrane by non-solvent induced phase inversion: relation between polymorphism and phase inversion, J. Membr. Sci. 550 (2018) 480–491.
[25] Y. Li, R. Yang, R. Zhang, B. Cao, P. Li, Preparation of thermally imidized polyimide nanofiltration membranes with macrovoid-free structures, Ind. Eng. Chem. Res. 59 (2020) 14096–14105.
[26] J.Q. Meng, C.H. Lau, Y.L. Xue, R. Zhang, B. Cao, P. Li, Compatibilizing hydrophilic and hydrophobic polymers via spray coating for desalination, J. Mater. Chem. A 8 (2020) 8462–8468.
[27] R.M. Zain, A.M. Razali, K.A.M. Salleh, R. Yahya, Image reconstruction of x-ray tomography by using image J platform, PLoS One 1799 (2017) 050010-1–050010-6.
[28] H. Sun, X. Yang, Y. Zhang, X. Cheng, Y. Xu, Y. Bai, L. Shao, Segregation-induced in situ hydrophilic modification of poly-(vinylidene fluoride) ultrafiltration membranes via sticky poly(ethylene glycol) blending, J. Membr. Sci. 563 (2018) 22–30.
[29] S.H. Yoo, J.H. Kim, J.J. Y, J. Won, Y.S. Kang, Influence of the addition of PVP on the morphology of asymmetric polyimide phase inversion membranes: effect of PVP molecular weight, J. Membr. Sci. 236 (2004) 203–207.
[30] S.L. Su, D.M. Wang, J.Y. Lai, Critical residence time in metastable region-a time scale determining the demixing mechanism of nonsolvent induced phase separation, J. Membr. Sci. 529 (2017) 35–46.

[31] H. Matsuyama, T. Maki, M. Teramoto, K. Kobayashi, Effect of PVP additive on porous polysulfone membrane formation by immersion precipitation method, Sep. Sci. Technol. 38 (2003) 3449–3458.
[32] M. Amirilargani, T. Mohammadi, Preparation and characterization of asymmetric polyethersulfone (PES) membranes, Polym. Adv. Technol. 20 (2009) 993–998.
[33] D.L. Wang, W.K. Teo, K. Li, Preparation and characterization of high-flux polysulfone hollow fiber gas separation membranes, J. Membr. Sci. 204 (2002) 247–256.
[34] L. Shi, R. Wang, Y. Cao, D.T. Liang, J.H. Tay, Effect of additives on the fabrication of poly (vinylidene fluoride-co-hexafluoropropylene) (PVDF-HFP) asymmetric microporous hollow fiber membranes, J. Membr. Sci. 315 (2008) 195–204.
[35] Y.H. Tang, Y.K. Lin, Q. Li, G. You, W.Z. Ma, X.L. Wang, Preparation and application of polyvinylidene fluoride membrane via thermally induced phase separation, J. Membr. Sci. 35 (2015) 98–107.
[36] M. Amirilargani, E. Saljoughi, T. Mohammadi, M.R. Moghbeli, Effects of coagulation bath temperature and polyvinylpyrrolidone content on flat sheet asymmetric polyethersulfone membranes, Polym. Eng. Sci. 50 (2010) 885–893.
[37] F. Zhou, W.J. Koros, Characterization of bore pressure change effects on Matrimid fiber performance in pervaporation of acetic acid and water mixtures, Chem. Eng. Sci. 61 (2006) 3736–3745.
[38] L.L. Xia, C.L. Li, Y. Wang, In-situ crosslinked PVA/organosilica hybrid membranes for pervaporation separations, J. Membr. Sci. 498 (2016) 263–275.
[39] T. Eljaddi, D.L.M. Mendez, E. Favre, D. Roizard, Development of new pervaporation composite membranes for desalination: theoretical and experimental investigations, Desalination 507 (2021), 115006.
[40] G.Z. Liu, J. Shen, Q. Liu, G.P. Liu, J. Xiong, J. Yang, W.Q. Jin, Ultrathin two-dimensional MXene membrane for pervaporation desalination, J. Membr. Sci. 548 (2018) 548–558.
[41] B. Liang, Q. Li, B. Cao, P. Li, Water permeance, permeability and desalination properties of the sulfonic acid functionalized composite pervaporation, Desalination 433 (2018) 132–140.
[42] X.W. Qian, N. Li, Q.Z. Wang, S.C. Ji, Chitosan/graphene oxide mixed matrix membrane with enhanced water permeability for high-salinity water desalination by pervaporation, Desalination 438 (2018) 83–96.
[43] R. Castro-Muñoz, Breakthroughs on tailoring pervaporation membranes for water desalination: a review, Water Res. 187 (2020), 116428.
[44] S.V.d.E.C. Dotremont, H. Vandommeleand, C. Vandecasteele, Concentration polarization and other boundary layer effects in the pervaporation of chlorinated hydrocarbons, Desalination 95 (1994) 91–113.
[45] E. Nagy, E. Kulcsar, The effect of the concentration polarization and the membrane layer mass transport on membrane separation, Desalin. Water Treat. 14 (2012) 220–226.
[46] N. Rafia, M.M. Beiragh, A.A. Babaluo, Concentration polarization in silica membranes, in: Current Trends And Future Developments on (Bio-) MembranesSilica Membranes: Preparation, Modelling, Application, And Commercialization, 2017, pp. 349–366.